# Kinetics of Aqueous Leaching and Carbonization of Steelmaking Slag

S.N. LEKAKH, C.H. RAWLINS, D.G.C. ROBERTSON, V.L. RICHARDS, and K.D. PEASLEE

Sequestration of carbon dioxide by steelmaking slag was studied in an atmospheric three-phase system containing industrial slag particles, water, and $CO_2$ gas. Batch-type reactors were used to measure the rate of aqueous alkaline leaching and slag particle carbonization independently. Four sizes of slag particles were tested for the Ca leaching rate in deionized water at a constant 7.5 pH in an argon atmosphere and for carbonate conversion with $CO_2$ bubbled through an aqueous suspension. Conversion data (fraction of Ca leached or converted to carbonate) were evaluated to determine the rate-limiting step based on the shrinking core model. For Ca leaching, the chemical reaction is the controlling mechanism during the initial period of time, which then switches to diffusion through the developed porous layer as the rate-limiting step. Carbonate conversion proceeded much slower than leaching conversion and was found to be limited by diffusion through the product calcium carbonate layer. The calculated value of diffusivity was found to be $5 \times 10^{-9}$ $cm^2/s$, which decreased by an order of magnitude with increasing carbonization conversion as a result of changing density of the product layer. The experimental data fit the shrinking core model well after correction for the particle specific surface area.

DOI: 10.1007/s11663-007-9112-8


## I. INTRODUCTION

THE United States produces 9 to 14 Mt of steelmaking slag annually, which represents approximately 10 to 15 wt pct of crude steel output.[1,2] Primary uses for steelmaking slag include high-quality mineral aggregate, Portland cement, soil conditioning, and pH neutralization of abandoned mine drainage.[3,4] The key factor prescribing slag use is the alkaline-earth metal (*e.g.*, Ca and Mg) oxide contents, which contribute to overall basicity and cementitious strength. However, as-produced steelmaking slag is chemically unstable as these oxides readily form hydroxides and carbonates through reaction with atmospheric gases. Both hydroxide and carbonate formation produce substantial mechanical swelling, leading to heave failure in confined construction applications; thus, many states dictate stockpile aging for 3 to 6 months prior to commercial use.[5,6]

Forced carbonation of steelmaking slag is a method to circumvent lengthy stockpile stabilization and provide the benefit of carbon dioxide sequestration. The conversion of CaO/MgO to carbonates serves both to stabilize the slag and to permanently capture and store the $CO_2$. Several research groups have started projects to determine the mechanisms involved in forced (accelerated) carbonation of steelmaking slag with the goal of using this material as a $CO_2$ sequestering agent. This work is an offshoot of a much larger-scale effort aimed at permanent geological sequestration of carbon dioxide with naturally occurring silicate or carbonate minerals.[7]

Huijgen and Comans measured the carbonation of steel slag in an autoclave reactor.[8,9] Particle size was found to have a strong effect on the extent of carbonation, while reactor temperature, reaction time, and $CO_2$ partial pressure had milder effects on Ca conversion. Carbonation was unaffected by stirring rate in the reactor, and Huijgen and Comans concluded that Ca diffusion through the product layer was the rate-limiting step. Huijgen and Comans concluded that their process can yield an 80 pct carbonation at relatively mild conditions ($< 38$ $\mu$m, 200 °C, 1.0 MPa $pCO_2$, 15 minutes). In comparison with naturally occurring wollastonite ($CaSiO_3$), steel slag was able to sequester 11 times more $CO_2$ at ambient temperature. Eloneva *et al.* investigated acetic acid leaching of slag for extraction of $Ca^{2+}$ to be used in producing precipitated calcium carbonate by reaction with $CO_2$ in a slurry crystallizer.[10] Leaching of slag resulted in extraction of 97 pct of the calcium ions compared to 38 pct extraction from wollastonite under the same conditions. Stolaroff *et al.* investigated the formation of dilute aqueous alkali-metal solution from steel slag that can be used to extract $CO_2$ from ambient air.[11,12] The rate and extent of calcium dissolution was found to be inversely related to

S.N. LEKAKH, Research Associate Professor of Metallurgical Engineering, C.H. RAWLINS, Graduate Researcher, D.G.C. ROBERTSON, Professor of Metallurgical Engineering, V.L. RICHARDS, Robert W. Wolf Professor of Metallurgical Engineering, and K.D. PEASLEE, F. Kenneth Iverson Steelmaking Chair, are with the Department of Materials Science and Engineering, Missouri University of Science & Technology, Rolla, MO 65409. Contact e-mail: chrnr9@mst.edu

Manuscript submitted July 9, 2007.

particle size and pH, and near terminal concentration of $Ca^{2+}$ may be reached in a few hours. Carbonation kinetics were not studied in this work; however, Huijgen and Comans suggest that Ca leaching and slag carbonation would occur simultaneously.

Extraction of $CO_2$ from steel manufacturing offgas using steelmaking slag is being studied to quantifying the extent and rate of carbonate formation under near-atmospheric aqueous conditions.[13] The value of $CO_2$ sequestration using steelmaking slag arises from its total carbonation potential and its ready availability as a co-product in steel production. A survey of industrial slags has found the CaO and MgO contents of BOF and EAF slags to average 30 to 50 wt pct and 10 to 12 wt pct, respectively.[13] Additionally, LMF slag contains 50 to 60 wt pct CaO and 10 to 12 wt pct MgO. The amount of slag produced per ton of steel is estimated at 75 to 150 kg for BOF, 65 to 80 kg for EAF, and 15 to 20 kg for LMF.[14] Production of a ton of steel generates 519 kg $CO_2$ carbon equivalent (CE) for BOF and 119 kg $CO_2$ CE for EAF. Assuming full stoichiometric conversion of CaO and MgO to carbonate, steelmaking slag has the potential to sequester 6 to 11 pct of the $CO_2$ generated from BOF production and 35 to 45 pct of the $CO_2$ generated from EAF production.[14]

While slag may contain a considerable fraction of CaO and MgO, these compounds are rarely present in pure form. The alkaline-earth metal oxides are primarily locked into silicate, aluminate, or ferrite phases. While the carbonation of these phases is highly exothermic (*e.g.*, $\Delta H^\circ_r = -116.2$ kJ/mole for $CO_2 + \frac{1}{2}Ca_2SiO_4 \rightarrow CaCO_3 + \frac{1}{2}SiO_2$), the reaction rates are very slow. Areas investigated to increase the reaction rate include fine grinding to increase surface area, increasing $CO_2$ partial pressure, increasing reactor temperature, and catalysis. The current study aims to quantify the reaction rate of steelmaking slag with $CO_2$ in aqueous systems operating at ambient pressure and temperature. Both the reaction rate of Ca leaching from slag into water and the direct carbonation of slag particles were investigated separately to understand the limiting mechanisms for the overall sequestration reaction.

## II. EXPERIMENTAL

Batch-reactor experiments were conducted to measure the reaction rate of industrial EAF and LMF slags with carbon dioxide in an aqueous system. The effect of slag particle surface area and alkaline earth metal oxide content on the extent of carbonization (wt pct CaO converted to $CaCO_3$) were investigated. These two parameters were selected in order to determine the hydrometallurgical model that best fits aqueous-assisted carbonation of steelmaking slag.

Three industrial slag samples (18 to 22 kg each) were studied: slag 1 was from an electric arc furnace (EAF), slag 2 from an Al-killed ladle metallurgy furnace (LMF), and slag 3 from a Si-killed LMF. The as-received slags 1 and 2 were gravel sized with most particles 2.5 to 7.5 cm in diameter, while slag 3 was a "falling slag" present as a fine powder. The slags were obtained within 24 hours of production and prior to on-site crushing and magnetic separation in order to ensure minimal reaction with the local atmosphere. Each slag sample was stored in separate double sealed plastic bins containing a bulk desiccant.

### A. *Slag Characterization and Sample Preparation*

Prior to beginning the reactor experiments, the chemical and physical characteristics of the slags were determined. X-ray fluorescence (XRF) spectroscopy was used to measure the elemental composition of each slag and assumes all components are present as oxides. X-ray diffraction (XRD) phase analysis (Scintag, Inc. PadX with Cu source, Cupertino, CA) was used to indicate the phase components of the slag samples.

To obtain fresh particle surfaces and sufficient amounts of slag particles across a range of size fractions, slags 1 and 2 were crushed in a laboratory jaw crusher followed by a roll crusher to pass a 6-mesh sieve size (3.35 mm). Slag 3 contained a high fraction of dicalcium silicate thus self-comminuted upon cooling and was used in the raw condition. Particle size distribution (PSD) was obtained using a United States mesh series of 8-in.-diameter sieves on a vibratory shaker with ~700-g samples produced by riffle splitting. After crushing and particle size analysis, four size fractions—45 to 75 $\mu$m, 150 to 250 $\mu$m, 420 to 590 $\mu$m, and 2300 to 3300 $\mu$m—were chosen for subsequent testing. As the slag-$CO_2$ reaction may be governed by particle surface area, the specific surface area ($m^2/g$) was determined for several fractions of the crushed slag samples using the BET gas sorption method (Quantachrome Corp., NOVA 1000, Boynton Beach, FL). Reflected light (RL) microscopy and scanning electron microscopy (SEM) with energy dispersive spectrometry (EDS) were used to study the surface topology, structure, and composition throughout different stages of the testing.

### B. *Reaction Kinetics*

Two sets of aqueous experiments were performed with the batch-type reactors. The first set of tests involved a simple stirred batch reactor to measure the leaching rate of calcium from the different size fractions of the slags. The leaching procedure was adopted from the work of Stolaroff.[12] Each leaching test was done in a 500 mL glass flask filled with 300 mL double de-ionized water and pH buffer TES (2-[(2-hydroxy-1,1-bis(hydroxymethyl)ethyl)amino]ethanesulfonic acid). The buffer was used to maintain the pH between 7.0 and 7.5. The buffered water was degassed by Ar bubbling and sealed under Ar positive pressure during the experiments. A quantity of slag (400 mg) was added such that the aqueous solution would be not saturated by $Ca^{2+}$ in the case of complete leaching. After a predetermined period of time, a 10 mL sample of the solution was taken from the reactor for each test and immediately filtered through 0.45-$\mu$m syringe filters to remove any suspended

solids, leaving only the dissolved fraction of $Ca^{2+}$. The ICP-OES spectrometry (PerkinElmer OPTIMA* 2000 DV) was used to measure the $Ca^{2+}$ concentration in the samples.

*OPTIMA is a trademark of PerkinElmer, Waltham, MA.

The second set of experiments involved measurement of the carbonization of slag particles in aqueous conditions. Thirty grams of each of the four size fractions from the slag samples were mixed with 250 mL of deionized water in a 500 mL flask. Standard grade $CO_2$ was introduced into the mixture through a 1.0-mm glass capillary tube. Each sample was allowed to react for a designated period of time, after which the $CO_2$ flow was stopped. The slurry mixture was filtered through 11-$\mu$m filter paper with a vacuum pump. The filtrand was dried at 180 °C and analyzed for carbon content using the combustion/IR method (LECO** CS600) or thermogravimetric analysis (TGA) in Ar atmosphere. Total weight loss up to ~600 °C gave the amount of hydroxide ($Ca(OH)_2$) formed and weight loss above this temperature was associated with the amount of carbonate ($CaCO_3$) formed.

**LECO is a trademark of LECO Corporation, St. Joseph, MI.

## III. RESULTS

### A. *Slag Characterization*

Table I lists the slag chemical compositions obtained by XRF, assuming all components to be oxides. The EAF slag 1 contained 32.1 pct CaO, while LMF slags 2 and 3 contained a higher, but nearly equal, percentage of CaO plus an $Al_2O_3/SiO_2$ amount that reflected their respective steel deoxidation practices. The XRD showed that the three slags listed in Table I contained primarily dicalcium silicate ($Ca_2SiO_4$) and tricalcium silicate ($Ca_3SiO_5$) with lesser amounts of akermanite ($Ca_2MgSi_2O_7$), $C_{12}A_7$ ($Ca_{12}Al_{14}O_{33}$), clinoenstatite ($MgSiO_3$), and magnesio-wustite ($MgFeO_2$). Only a minor amount of free periclase (MgO) and lime (CaO) was present, showing the alkaline earth metal oxides are primarily tied up as silicates, aluminates, and ferrites. Minor amounts of free alumina ($Al_2O_3$), wustite (FeO), and silica ($SiO_2$ quartz) were also found; however, these do not contribute to carbon dioxide sequestration.

**Table I. Steelmaking Slag Composition (Weight Percent)**

| Sample | 1 | 2 | 3 |
|---|---|---|---|
| Type | EAF | LMF Al killed | LMF Si killed |
| CaO | 32.1 | 49.9 | 51.3 |
| $SiO_2$ | 19.4 | 4.5 | 28.3 |
| $Al_2O_3$ | 8.6 | 32.3 | 4.9 |
| $TiO_2$ | 0.4 | 0.3 | 0.3 |
| MgO | 9.4 | 4.3 | 4.3 |
| MnO | 6.8 | 0.8 | 1.3 |
| $Fe_xO_y$ | 26.4 | 6.3 | 5.5 |
| $SO_3$ | 0.6 | 1.0 | 1.6 |

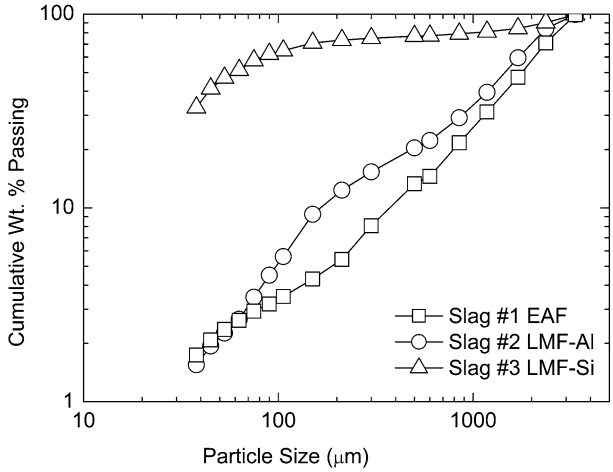


Fig. 1—Particle size analysis of slags 1 and 2 after crushing and slag 3 as received.

Figure 1 shows the particle size analysis of slags 1 and 2 after crushing, along with slag 3 in the raw state. Slags 1 and 2 have very similar PSD after crushing; however, slag 3 is much finer. The measured specific surface area ($m^2/g$) was compared with the calculated surface area for hypothetical smooth uniform spherical particles. The measured surface area of LMF slag particles was an order of magnitude larger than that calculated for uniform spheres, while the EAF slag particles had two orders of magnitude greater surface area because slag particles had internal and external porosity.

### B. *Reaction Kinetics*

#### 1. *Ca Leaching*

Figure 2 shows the effect of particle size, solution temperature, and slag composition on the aqueous extraction rate of $Ca^{2+}$ from slag samples. The aqueous solution was maintained at a constant pH of 7.5 throughout each test. Figure 2(a) shows the amount of $Ca^{2+}$ dissolved up to 24 hours for four size fractions of slag 2 (LMF slag with 49.9 pct CaO). The percentage of calcium dissolved was calculated from the concentration of $Ca^{2+}$ in the solution and the total amount of Ca (as CaO) added to the batch reactor. The particle size (*i.e.*, surface area) had a dominant influence on the amount of calcium leached. During the first hour, approximately 33 pct of the calcium was leached from the 45- to 75-$\mu$m fraction, while less than 5 pct of the calcium was leached from the 2300- to 3300-$\mu$m fraction after 24 hours. The effect of temperature on Ca leaching, as shown in Figure 2(b), was more pronounced during the first few hours, but after 3 hours, the leaching rate (pct Ca dissolved/time) became similar for the two temperatures tested. Figure 2(c) shows the absolute value of $Ca^{2+}$ (ppm) in solution *vs* time to provide a comparison of leaching different types of slags with the same size particles (150 to 200 $\mu$m). EAF slag 1 has less

CaO than LMF slag 2 (32.1 pct *vs* 49.9 pct), but a higher surface area. The leaching rate during the first 100 minutes was higher for slag 1 due to the increased surface area; however, the overall amount of calcium dissolved after 24 hours is significantly higher for slag 2 due to the higher starting CaO concentration.

The changes in particle morphology and composition during leaching were examined using SEM/EDS and XRD analysis. The leaching of Ca from a slag particle started at the slag surface including internal pores connected to the particle's external surface. Figure 3 shows the porous layer remaining on the external surface (Figure 3(a)) and internal surface (Figure 3(b)) after leaching of slag 1. The EDS analysis of the unreacted core and the surface after leaching showed that selective dissolution takes place. The concentration of Ca in the unreacted core is very high (44.5 wt pct), while the Ca at the surface after leaching is depleted (0.33 wt pct). Selective leaching of the Ca from the surface leaves behind an undissolved layer of mixed

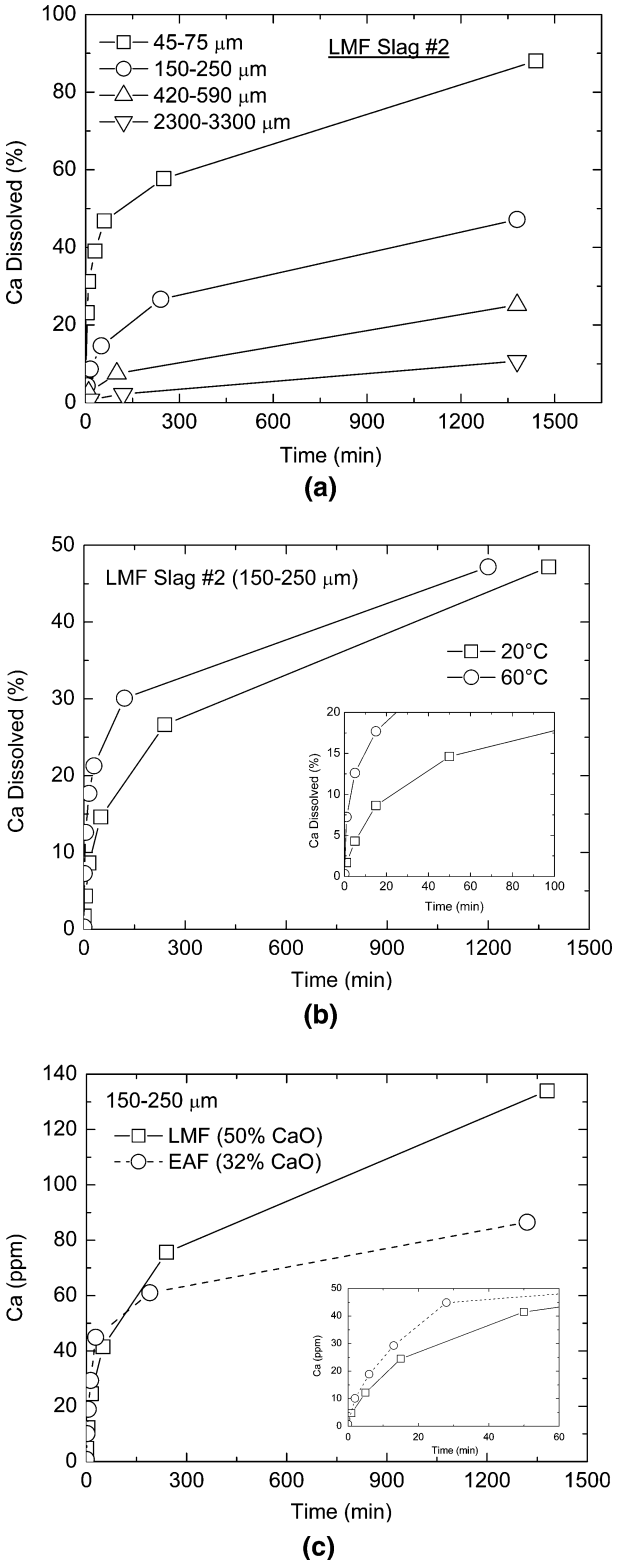


Fig. 2—Effect of (*a*) particle size, (*b*) temperature, and (*c*) CaO concentration in slag on the aqueous leaching rate of calcium.

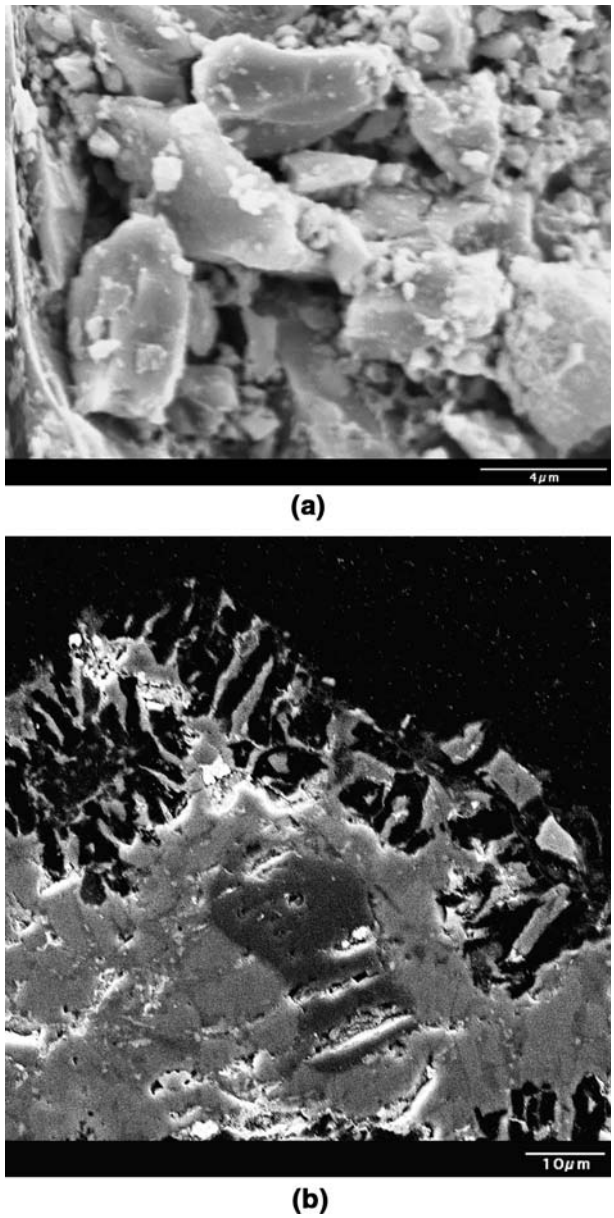


Fig. 3—(*a*) External surface and (*b*) cross-sectional images of slag 1 after leaching.

(Al, Fe, Mn, Mg) oxides in different phases than the original slag. The XRD analysis showed that after 24 hours leaching, the alumino-calcium-silicate phase was eliminated.

2. *Slag Carbonization*

The degree of carbonization *vs* log (time) for four size fractions of slags 1 and 2 is presented in Figure 4. For both slags, the particle size is the dominant influence on the amount of carbonization. Comparing the 0.06-, 0.2-, 0.5-, and 1.25-mm average particle sizes tested for slag 1 (Figure 4(a)) showed that the time to reach 6 pct carbonization was approximately 20, 800, 1500, and 4200 minutes, respectively. The data for slag 2 (Figure 4(b)) showed the same relationship between particle size and degree of carbonization; however, the overall carbonization amount is less than that of slag 1 for all particle sizes. Measurement of the degree of carbonization is less precise than that of the Ca leaching tests due to the small amount of initial carbon present in the slag and the nature of carbon measurement with TGA compared to aqueous Ca ion measurement with ICP.

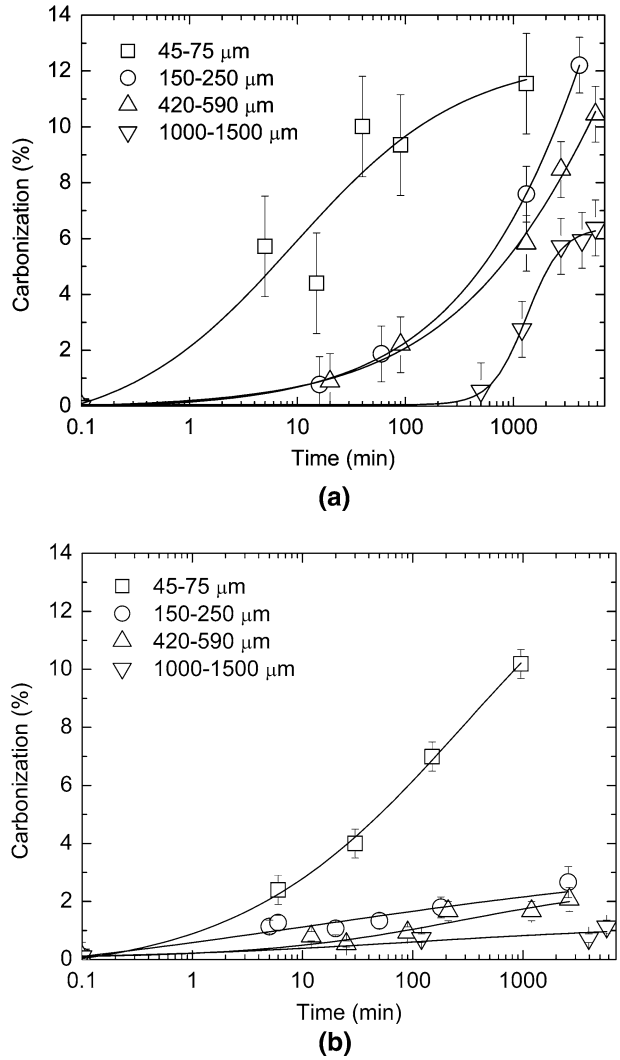


Fig. 4—Degree of carbonization *vs* time for four size fractions of (*a*) slag 1 and (*b*) slag 2.

Morphological analysis of the resultant carbonate layers is shown in Figure 5. Because slag particles exhibit a highly porous structure, interconnected channels allow surface reactions to take place deep inside the

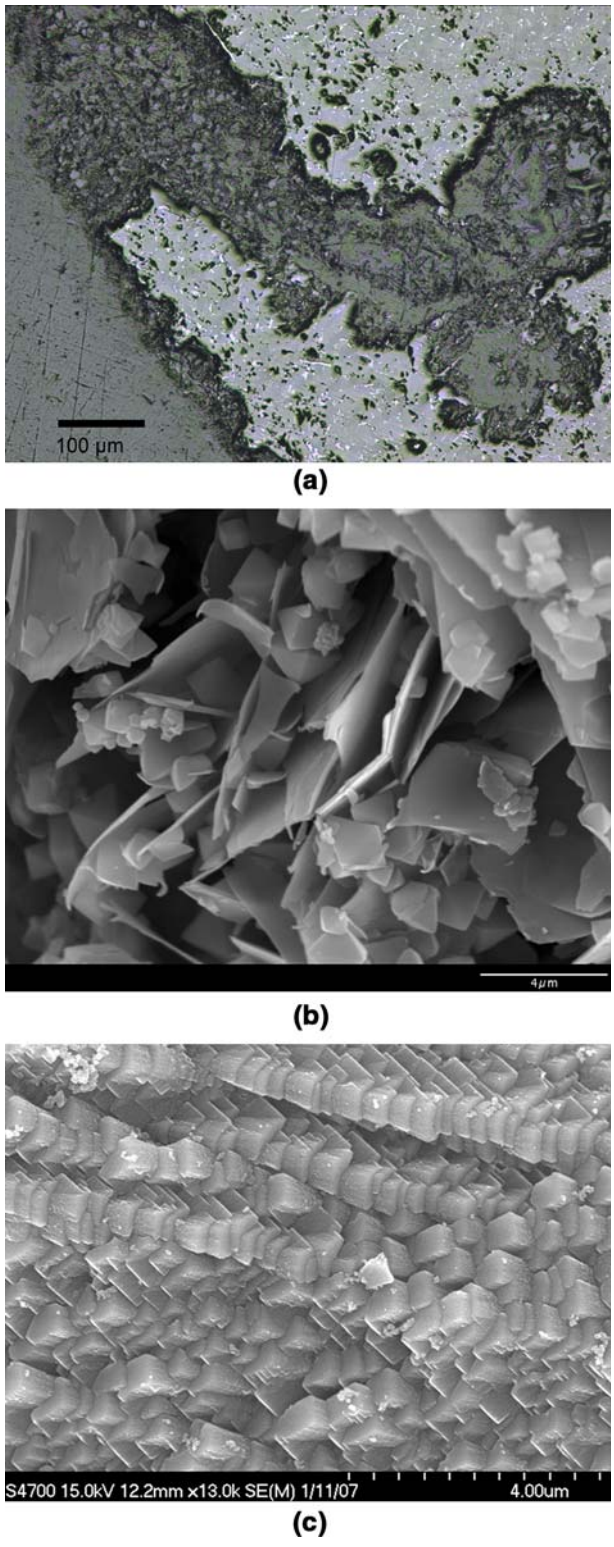


Fig. 5—(*a*) Optical image of slag 2 particle showing the cross section of a pore. SEM image of (*b*) the external surface carbonate layer and (*c*) the pore surface carbonate layer.

**Table II. Specific Surface Area ($m^2/g$) of Slag after Aqueous Treatment**

| | Condition | | |
|---|---|---|---|
| Slag (0.15 to 0.25 mm) | Initial | $CO_2$ Treated | Leached |
| EAF 1 | 1.13 | 12.6 | 5.42 |
| LMF 2 | 0.092 | 4.4 | NA |

slag particle. A cross-sectional sample of a 0.5-mm particle from slag 2 (Figure 5(a)) after 48 hours carbonization treatment showed a 10- to 20-$\mu$m-thick carbonate layer on the external surface (dark region) extending into the pores, which are up to 100-$\mu$m diameter. The SEM analysis showed that the carbonate layer on the external surface of slag 2 consisted of platelike crystals in a random high-porosity structure with 1- to 3-$\mu$m openings (Figure 5(b)). The EDS analysis of the plates showed them to be composed primarily of Ca, O, and C, indicating a calcium carbonate composition. Pores connected to the slag surface through channels were exposed by crushing the particles prior to SEM analysis. The pore surfaces showed a reaction layer made of overlapping plates of calcium carbonate packed very close together, thus having a higher bulk density (Figure 5(c)).

Two different types of reactions between steelmaking slag and water were experimentally tested. The first reaction involved simple leaching of $Ca^{2+}$ ions from slag into nearly pure water with constant pH and surrounded by an inert atmosphere. No hydrous $CO_2$ or other impurities were present to react with the calcium ions. In contrast, the second type of reaction allowed for the formation of calcium carbonate due to saturation of aqueous solution with $CO_2$. The progress of both types of reactions changed the specific surface area of the solid slag particles, as shown in Table II. Leaching increased the specific surface area by increasing the surface porosity as a result of selective dissolution of the Ca bearing phases (Figure 3), while the carbonization reaction increased the specific surface area by the production of a highly irregular product layer (Figure 5).

## IV. DISCUSSION

The shrinking core model is typically used for analysis of heterogeneous solid-fluid reactions involving particles and for the determination of the rate-limiting mechanism. A description of this model can be found elsewhere.[15] Application of this model to slag carbonization reveals that the reaction steps must include (1) mass transport of the aqueous carbonic acid ions through the liquid boundary layer surrounding the particle, (2) diffusion of the reacting ions through the pores in the product layer ($CaCO_3$) accreted on the slag particle surface, and (3) the reaction of calcium ions at the solid surface with aqueous carbonic acid ions $\left(HCO_3^- \text{ and } CO_3^{2-}\right)$. For the Ca ion leaching-only process, the reaction steps are (1) the surface reaction of Ca bearing phases with water, (2) mass transport of the $Ca^{2+}$ through the porous surface structure developed from selective leaching, and (3) mass transport of the calcium ion through the liquid boundary layer. According to the shrinking core model, originally developed for dense spherically shaped uniform sized particles, each reaction step possesses a specific time dependence, which has a characteristic proportionality to the particle surface area and solution temperature. The measured effective diffusivity was approximately $10^{-9}$ to $10^{-10}$ $cm^2/s$, while the diffusivity in the bulk liquid is on the order of $10^{-5}$ $cm^2/s$; thus, mass transport through the liquid boundary layer was neglected as the rate-limiting step. The slurry was intensively mixed with magnetic stirring to maintain a uniform concentration in the bulk solution. Therefore, the chemical reaction between the solid and liquid-ionic species or diffusion through the pores in the product layer can be assumed to control the rate of the processes studied.

When the diffusion of the reactants through the product layer is rate limiting, Eq. [1] gives the dependence of the molar transport of bulk fluid reactant $A$ ($-dN_A/dt$, mol/s) through the product layer at a radius $r$ (cm) and effective diffusivity $D_e$ ($cm^2/s$).[15] The term $C_A$ ($mol/cm^3$) is the concentration of the bulk reactant, which is a function of radius. At the radius of the unreacted core, $C_A$ is zero, while at the outer radius of the product layer (in contact with surrounding fluid), $C_{Ab}$ is the concentration of the reactant ions in the bulk fluid.

$$\frac{-dN_A}{dt} = (4\pi r^2)\left(-D_e \frac{dC_A}{dr}\right) \quad [1]$$

Solving for the reaction time $t$ (seconds), as shown in Eq. [2], shows dependence on the particle initial radius $R$ (cm), the unreacted core radius $r_c$ (cm), the molar density of the solid $\rho_B$ ($mol/cm^3$), and the stoichiometric coefficient $b$.[15] In regard to particle size, the reaction time to a fixed level of completion is a function of the square of the particle radius.

$$t = \frac{\rho_B R^2}{6bD_e C_{Ab}}\left[1 - 3\left(\frac{r_c}{R}\right)^2 + 2\left(\frac{r_c}{R}\right)^3\right] \quad [2]$$

When the chemical reaction between the solid and liquid-ion species is rate limiting, Eq. [3] gives the relationship between surface area, molar transport of bulk fluid reactant $A$, rate constant $k_r$ (cm/s), and concentration of bulk reactant.

$$-\frac{1}{4\pi r^2}\frac{dN_A}{dt} = k_r C_A \quad [3]$$

Rearrangement and integration of Eq. [3] provides the reaction time as a function of the parameters shown in Eq. [4]. In regard to particle size, the reaction time is a function of the particle radius to the first power.

$$t = \frac{\rho_B}{bk_r C_{Ab}}(R - r_c) \quad [4]$$

For determination of the rate controlling step (*i.e.*, that governing the leaching rate of Ca or the degree of carbonization *vs* time), the influence of particle size and

solution temperature was analyzed. Particle size effect on the time to reach the same level of $Ca^{2+}$ in the solute (Figure 2) or the time to reach the same level of carbonization (Figure 4) was analyzed for the respective experiments. If the time has a squared dependence particle size, then the reaction is likely governed by product layer diffusion (Eq. [2]); however, if the time has a linear dependence on particle size, then the reaction is governed by the chemical reaction (Eq. [4]). The time dependence for both leaching and carbonization is analyzed based on calcium conversion, $X_{Ca}$, as a fraction of reacted calcium initially present in the slag.

## A. *Ca Leaching*

Analysis of experimental data for slag 2 (Figure 2(a)) showed that both mechanisms were involved sequentially during Ca leaching from steelmaking slag. During the initial stage (*i.e.*, to 0.07 conversion), the reaction time showed linear proportionality to particle size (Figure 6(a)). This supports a chemical reaction controlled model whereby solid CaO dissolves into $Ca^{2+}$ ions in the water. As the dissolution reaction progressed to 0.18 conversion, a porous surface structure developed, as shown in Figure 3, resulting in a tortuous path for the ions to travel. Subsequent diffusion through this structure became the rate-limiting step, as shown by the square root proportionality of the reaction time to particle size (Figure 6(b)).

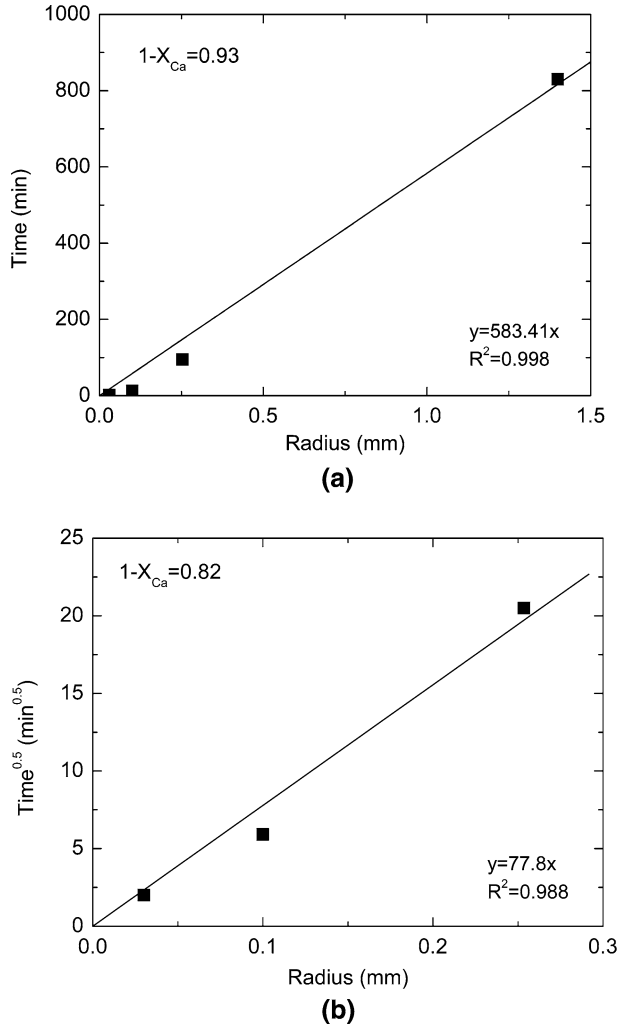


Fig. 6—Time dependence with particle size for Ca leaching from slag 2 for the (*a*) initial stage and (*b*) progressive stage.

Comparison of the experimental data for slag 2 (Figure 2(a)) with Eqs. [2] and [4] allows for direct correlation. Figure 7 shows a plot of the experimental data (45- to 75-$\mu$m particles) compared to the diffusion and reaction equations. A combination of the two equations shows that the experimental data fit well to a chemical reaction controlled mechanism up to ~0.3 conversion (60 minutes), and then switches to a combination of chemical reaction and porous diffusion layer control to the terminal conversion of 0.63.

Each reaction mechanism has a different sensitivity to the solution temperature. In the case studied, increasing the temperature of the aqueous solution enhanced Ca leaching at the initial reaction time period (Figure 2(b)). While the rate of dissolution increased significantly with temperature during the initial period, the rate of leaching at the end of the test did not differ greatly between 20 °C and 60 °C. This is because the solution temperature affects the rate of the chemical reaction more than it does the rate of diffusion.

In Figure 2(c), EAF slag 1 showed a higher Ca dissolution rate during the initial period even with a lower Ca concentration in slag when compared to LMF slag 2. This is inconsistent with a simple shrinking core model based on uniform smooth solid spheres. Correction of this model can be made by substituting an effective particle size, which is based on the measurement of specific surface area. Slag 1 had ~10 times the surface area of slag 2 for the same particle size. The much higher surface area led to an increased Ca dissolution rate during the initial period. However, as the Ca rapidly dissolved, the amount of Ca left in the slag decreased, providing less gradient to maintain the

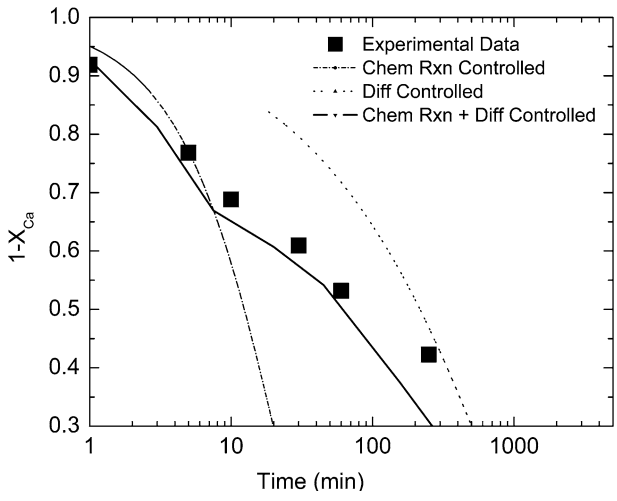


Fig. 7—Comparison of experimental data for Ca leaching from slag 2 (45- to 75-$\mu$m particle size) with chemical and diffusion reaction control mechanisms.

high dissolution rate. Slag 2 had 55 pct more Ca to start with; thus, it was able to maintain a higher gradient compared to the bulk solution, resulting in an overall higher amount of Ca leached.

### B. *Slag Carbonization*

The slag carbonization data were analyzed in a similar manner to determine the controlling reaction mechanism. Figure 8(a) shows the time required to achieve 0.02 conversion (carbonate reaction) for four particle sizes of slags 1 and 2. Conversion was heavily dependent on particle size and showed proportionality to the square root of time, indicating that product layer diffusion was the rate controlling step. The layer of calcium carbonate formed on the surface (Figure 5) retarded the diffusion of carbonic acid ions into the slag particle. The different slopes exhibited by the two slags reflected the effect of true surface area. The effective diameters, calculated from specific surface measurements on the assumption of uniform spherical particles, were used to recalculate the curves shown in Figure 8(b), bringing both curves into congruence.

According to the shrinking core model, if product layer diffusion is the limiting mechanism (Eq. [2]), conversion should exhibit a dependence on the square root of reaction time. Figure 9(a) shows the experimental data for conversion of slag 1 *vs* [time$^{0.5}$]. During the initial reaction period (*i.e.*, to 0.03 conversion), the experimental results closely match the theoretical model. As the product layer increases in thickness, the reaction tends to decelerate. The changing density of the carbonized layer (Figure 5(a)) was not considered in this model and is a possible explanation for the decrease in reaction rate. Equation [2] was solved numerically by changing the effective diffusivity (*i.e.*, for increased product layer thickness) for the three conversion periods shown in Figure 9(a) ($<0.03$, 0.03 to 0.10, and $>0.10$) to allow the fraction converted to match the square root relationship. The experimental data were fit to the resulting equations to yield a diffusion coefficient that changed from $5 \times 10^{-9}$ cm$^2$ s$^{-1}$ at an initial period of

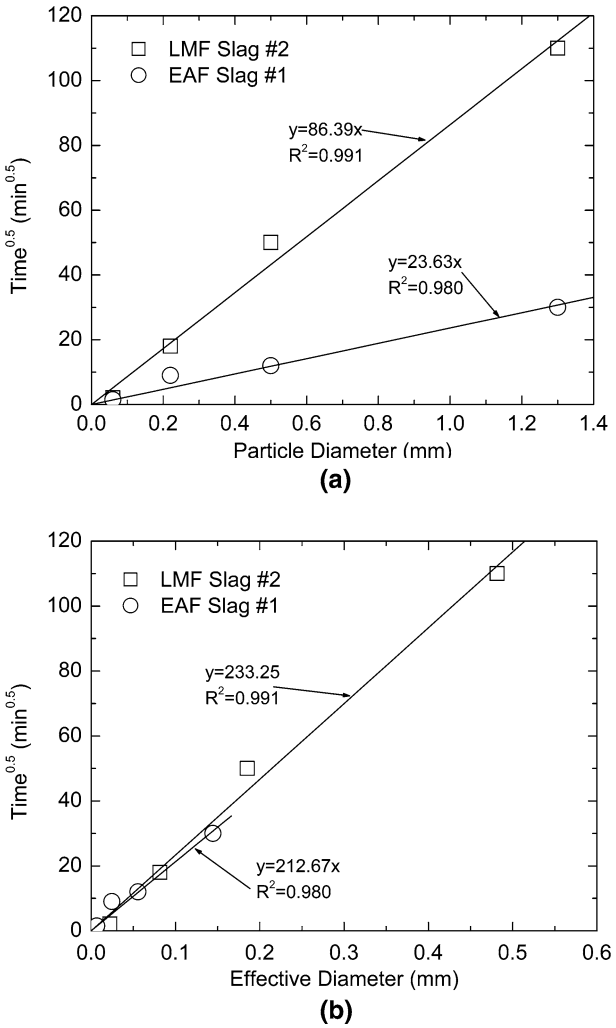


Fig. 8—Diffusion limiting model for the slag carbonization reaction at 0.02 Ca conversion using the (*a*) real particle diameter and (*b*) effective particle diameter.

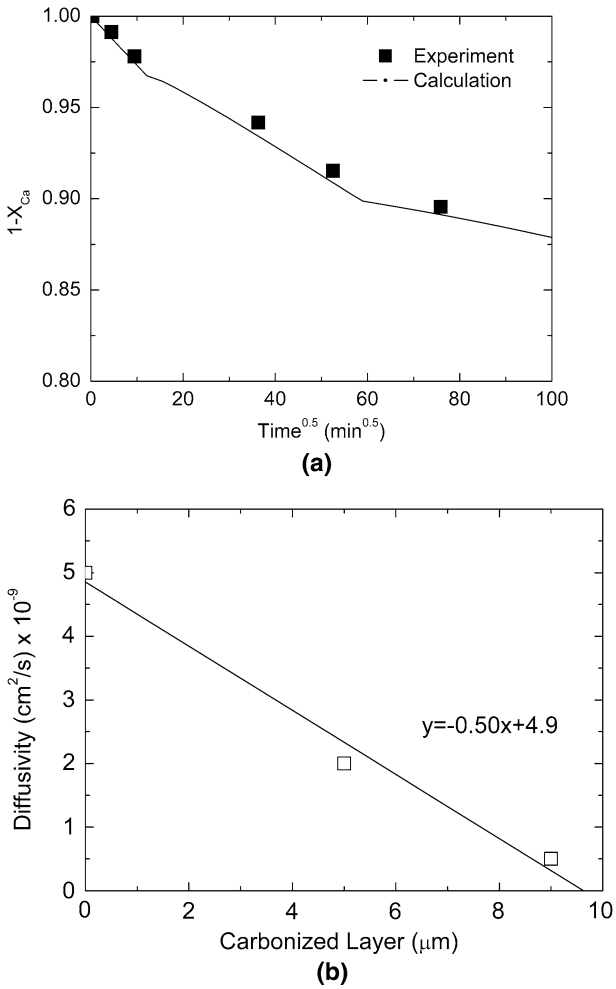


Fig. 9—(*a*) Comparison of calculated and experimental data for the carbonization of slag 1 with 0.5-mm average particle diameter and (*b*) dependence of diffusivity on the thickness of the carbonized layer.

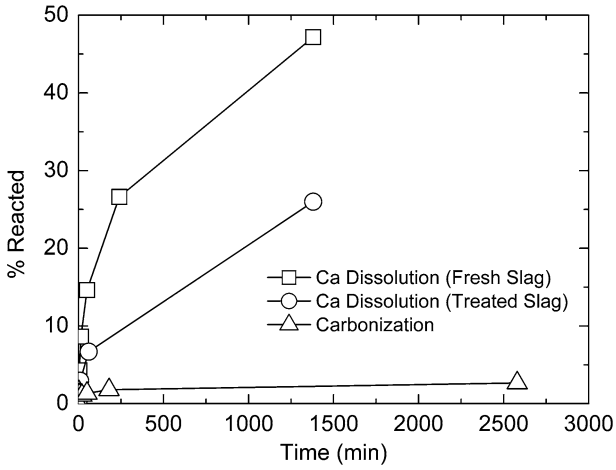


Fig. 10—Comparison of carbonized and leached Ca from fresh and stabilized LMF slag 2 in aqueous solutions.

time to $5 \times 10^{-10}$ cm$^2$ s$^{-1}$ when carbonate layer was formed, as shown in Figure 9(b).

Finally, data for the rate of Ca leaching were compared to data for the rate of Ca carbonization for the same slag. In both cases, some amount of calcium from the slag reacted with the aqueous solution; however, the rate of these reactions significantly differed due to the mechanisms and limiting steps involved. In the slag leaching test, Ca ions dissolved from the slag into the unsaturated aqueous solution. The limiting step was the diffusion of calcium ions through the developed porous layer. An additional Ca leaching test was performed on slag 2 ($< 200$ $\mu$m), which had been preliminary partially carbonized. Figure 10 shows the percentage of reacted Ca from slag (leached or carbonized) *vs* reaction time. The comparison illustrates that slag carbonization proceeds slower than Ca leaching. In addition, the calcium carbonate product layer inhibits the Ca leaching process. The experimental data and kinetic parameters obtained will be used for modeling an industrial prototype reactor that can be used for sequestration of carbon dioxide with steelmaking slag.

## V. CONCLUSIONS

Carbon dioxide sequestration with steelmaking slag was studied in a three-phase batch-system containing industrial slag, water, and $CO_2$ gas at ambient temperature and pressure. The reaction rates of aqueous Ca leaching and direct carbonization were quantified independently to yield the reaction parameters and rate-limiting mechanisms, as listed subsequently.

1. The specific surface area of slag particles is increased by leaching or carbonization. Selective dissolution of the Ca-bearing phase results in increased surface porosity, while carbonization produces overlapping plates of $CaCO_3$ product layer that create a highly irregular surface.
2. Both Ca leaching and carbonization were analyzed using the shrinking core model. The experimental data for both processes fit this model well, after correction for effective particle size, which is based on the measured specific surface area.
3. Analysis of Ca-leaching shows a linear proportionality to particle size during the initial stage (to 0.30 conversion), supporting a chemical reaction controlled model (CaO dissolution). The later stage of leaching is controlled by diffusion of the $Ca^{2+}$ ions through the resulting porous surface layer, as shown by square-root proportionality of reaction time to particle size.
4. Increasing the leachate temperature from 20 °C to 60 °C (at atmospheric pressure) enhanced the Ca-leaching rate during the initial period time; however, the terminal amount of Ca leached after 24 hours did not differ greatly (47 pct *vs* 50 pct).
5. Carbonate conversion is heavily dependent on particle size, and the reaction is limited by product layer diffusion. The calculated value of diffusivity decreased by an order of magnitude from the initial value of $5 \times 10^{-9}$ cm$^2$/s, as a result of the changing density of the product layer.
6. Carbonate conversion proceeded slower than did leaching conversion; however, both processes were inhibited by the calcium carbonate product layer.

## ACKNOWLEDGMENTS

This article was prepared as an account of work sponsored by the United States Department of Energy, in cooperation with the American Iron and Steel Institute (AISI) and its participating companies, under Agreement No. DE-FC36-97ID13554. Such support does not constitute an endorsement by DOE or AISI of the views expressed in this article. The authors also acknowledge the support of DOFASCO, Gallatin Steel, Hylsa, IPSCO, Mittal Steel, Praxair, Nucor, Timken Company, and US Steel.

## REFERENCES

1. U.S. Department of the Interior, U.S. Geological Survey, Minerals Information, Jan. 12, 2005, http://www.minerals.usgs.gov/minerals/pubs/commodity/iron_&_steel_slag/.
2. H.G. van Oss: *U.S. Geological Survey Minerals Yearbook, 2003*, 69.1–69.3, June 30, 2005, http://www.minerals.usgs.gov/minerals/pubs/commodity/iron_&_steel_slag/islagmyb03.pdf.
3. National Slag Association [brochure], June 30, 2005, http://www.nationalslagassoc.org/PDF_files/SSPremAgg.pdf.
4. D.W. Lewis: Report No. MF 182-6, National Slag Association, Pleasant Grove, UT.
5. Missouri Department of Transportation, Apr. 14, 2004, http://www.modot.org/business/standards_and_specs/nov2004specbook/Sec1002.pdf.
6. P.S. Kandhal and G.L. Hoffman: *Transport. Res. Rec.*, 1997, No. 1583, pp. 28–36.
7. K.S. Lackner: *Ann. Rev. Energy Environ.*, 2002, vol. 27, pp. 193–232.
8. R.N.J. Comans and W.J.J. Huijgen: *Proc. 32nd Int. Geological Congr.*, Session G15.05, Florence, Italy, Aug. 23, 2004.
9. W.J.J. Huijgen, G.-J. Witkamp, and R.N.J. Comans: *Environ. Sci. Technol.*, 2005, vol. 39 (24), pp. 9676–82.

10. S. Eloneva, S. Teir, C.-J. Fogleholm, and R. Zevenhoven: *Proc. 4th Nordic Minisymp. on Carbon Dioxide Capture and Storage*, Espoo, Finland, Sept. 8–9, 2005.
11. J.K. Stolaroff, G.V. Lowry, and D.W. Keith: Fall Meeting, San Francisco, CA, Dec. 8–12 2003, *EOS Trans. AGU*, 2003, vol. 84 (46).
12. J.K. Stolaroff, G.V. Lowry, and D.W. Keith: *Energy Conserv. Manag.*, 2005, vol. 46 (5), pp. 687–99.
13. C.H. Rawlins, V.L. Richards, K.D. Peaslee, and S.N. Lekakh: *Proc. AISTech 2006 Conf.*, Cleveland, OH, May 1–4, 2006.
14. C.H. Rawlins, V.L. Richards, K.D. Peaslee, and S.N. Lekakh: *Steel Times Int.*, 2006, vol. 30 (7), pp. 25–26.
15. K.N. Han: *Fundamental of Aqueous Metallurgy*, Society for Mining, Metallurgy, and Exploration Inc, Littleton, CO, 2002, pp. 129–40.